Molecular Packing and Molecular Dynamics Study of the Transferability of a Generalized Nitramine Intermolecular Potential to Non-Nitramine Crystals

Dan C. Sorescu,[†,‡] Betsy M. Rice,[§] and Donald L. Thompson*[,†]

Department of Chemistry, Oklahoma State University, Stillwater, Oklahoma 74078, and The U. S. Army Research Laboratory, Aberdeen Proving Ground, Maryland 21005

Received: September 23, 1998; In Final Form: December 30, 1998

We have analyzed the transferability of a previously proposed intermolecular potential for nitramine crystals to reproduce the experimentally determined crystal structures (within the approximation of rigid molecules) of 51 nitro compounds. These compounds include different types of acyclic, monocyclic, and polycyclic molecules. It is shown that this potential model accurately reproduces the experimentally determined crystallographic structures and lattice energies for the majority of these crystals. The best agreement with experimental structural and energetic data is obtained when the electrostatic charges have been determined using ab initio methods that include electron correlation effects, namely MP2 and B3LYP. The use of the electrostatic charges calculated at the Hartree−Fock level results in large differences between the predicted and the experimental values of the lattice energies. This difference can be significantly decreased by scaling the electrostatic charges with a general factor without introducing significant variations of the predicted crystallographic parameters. Further testing of the proposed intermolecular potential has been done by performing isothermal−isobaric molecular dynamics (MD) simulations over the temperature range 100−450 K, at atmospheric pressure, for the monoclinic phase of the 2,4,6-trinitrotoluene (TNT) crystal and for the polymorphic phase I of the pentaerythritol tetranitrate (PETN I) crystal. In each case, the results show that throughout the MD simulations the average structures of the crystals maintain the same space group symmetry as the one determined experimentally and there is a good agreement between the calculated crystallographic parameters and the experimental values. The thermal expansion coefficients calculated using the present model indicate an overall anisotropic behavior for both TNT and PETN I, with a thermal isotropy for PETN I along cell directions *a* and *b*.

I. Introduction

The work presented here is the fifth in a series of studies[1−4] that investigates the degree to which an intermolecular potential energy function that was developed to describe a single molecular crystal can be extended to describe crystal structures of other similar systems. The function, consisting of atom−atom (6-exp) Buckingham terms and electrostatic interaction terms in the form of partial charges associated with the atoms, was parametrized to reproduce the experimental crystal structural information of the α-form of the solid explosive, RDX (hexahydro-1,3,5-trinitro-1,3,5-*s*-triazine).[1] The parametrization of the function was done such that molecular packing calculations (MP) reproduced the experimental structure of the crystal and its lattice energy with the electrostatic charges determined at the second-order Møller−Plesset 6-31G** level. This intermolecular potential was also used in isothermal−isobaric molecular dynamics (NPT-MD) calculations at ambient pressure for temperatures ranging from 4.2 to 325 K. The results of the simulations are in good agreement with experiment, with the lattice dimensions being within 2% of experiment and almost no rotational or translational disorder of the molecules in the unit cell. The space group symmetry was maintained throughout the simulations. Thermal expansion coefficients were also determined for the model and are in reasonable accord with experiment.

The recently developed explosive 2,4,6,8,10,12-hexanitrohexaazaisowurtzitane (HNIW) can be described as a bridged pair of RDX molecules, suggesting that the intermolecular forces for HNIW might be similar to those of RDX. To explore this possibility, we performed MP and NPT-MD simulations[2] for three of the polymorphs of HNIW (β-, ϵ-, and γ-phases) at ambient pressure and over the temperature range 4.2 to 425 K using the form of potential used in the RDX study.[1] The parameters for the Buckingham terms remained unchanged, and the Coulombic interaction terms between electrostatic charges were determined from fits to ab initio electrostatic potentials calculated for the individual molecules corresponding to the different polymorphs, whose atoms are arranged in the experimental configurations. We found that the potential predicts the right order of stability for different phases of HNIW ($\epsilon > \beta > \gamma$) crystals in agreement with experimental measurements.[4] At 300 K, the average lattice dimensions agree very well with experimental values, with the corresponding differences for the individual cell edge lengths being no more than 1.0% for the ϵ-polymorph, 0.9% for the β-polymorph, and 2.5% for the γ-polymorph. For the ϵ- and γ-phases, the variations of the unit cell angle β from the experimental values are 1.3% and 0.1%, respectively, while the other two angles of the unit cell remain approximately equal to 90°. For the β-phase, all three crystal-

[†] Oklahoma State University.
[‡] Current mailing address: Department of Chemistry, University of Pittsburgh, Pittsburgh, Pennsylvania 15260.
[§] The U.S. Army Research Laboratory.

10.1021/jp983847e CCC: $18.00
Published on Web 02/10/1999

lographic angles remain approximately equal to 90°, in agreement with experiment. Additionally, little rotational or translational disorder occurs throughout the simulations. The largest deviation between experimental values and predictions of molecular orientation occurs for γ-HNIW; the predicted value of one of the Euler angles defining the molecular orientation deviates by 4.4° from the experimental value.

We next performed MP and NPT-MD simulations at atmospheric pressure and different temperatures for the β-, α-, and δ-phases of another nitramine crystal, the explosive 1,3,5,7-tetranitro-1,3,5,7-tetraazacyclooctane (HMX).[3] Again, the Buckingham terms were those used in the RDX study, and the only differences in the potential are the Coulombic interactions between electrostatic charges centered on the atoms. At room temperature, the predicted average lattice dimensions of the β-phase are within 0.7% of the experimental values, and at 376 K, the differences of the lattice dimensions for the α-phase are within 2.6%. The differences for the δ-phase are within 4.4% at 433 K. In addition, for all three phases, the angles of the unit cell remain close to the experimental values with the maximum difference of 2.5% for the β angle of β-HMX. However, it should be pointed out that in the cases of α- and δ-HMX, the crystallographic data were determined at $T = 295$ K, although this temperature is outside the stability range of these two phases. There are no significant displacements of the molecular center of mass or increase of the degree of rotational disorder for the three phases. The largest difference between experiment and predictions of molecular orientation is for one of the Euler angles for α-HMX; the predicted average value is 3.8° larger than the experimental value. Besides the geometrical parameters, the calculated lattice energies for the three phases support the experimentally determined polymorph stability ranking ($\beta > \alpha > \delta$) given by McCrone.[6] Moreover, for the β- and δ-phases, where experimental values for the heats of sublimations have been determined, the predicted lattice energies are in very good agreement with the experimental values.

More recently, we have extended our investigations of the transferability properties of this interaction potential to a collection of 30 nitramine crystals.[4] The crystals are composed of monocyclic, polycyclic, and acyclic nitramine molecules. The molecules associated with the nitramine crystals were chosen as representative examples of acyclic and cyclic nitramines. In the latter case, we have included different types of mono- and polycyclic nitramines, particularly crystals of importance in energetic materials. For most of the crystals, the predicted structural lattice parameters differ by less than 2% from the experimental structures with small rotations and practically no translations of the molecules in the asymmetric unit cell.

In the present study, we extend our investigations beyond the case of nitramine crystals. For this purpose, we have performed MP calculations on 51 crystals comprising a wide variety of compounds such as nitroalkanes, nitroaromatics, nitrocubanes, polynitroadamantanes, polynitropolycycloundecanes, polynitropolycyclododecanes, hydroxynitro derivatives, nitrobenzonitriles, nitrobenzotriazoles, and nitrate esters such that a comprehensive test to our potential can be achieved. We have been particularly interested to see if the geometrical and the known energetic parameters for these types of crystals can be reproduced accurately by the proposed intermolecular potential.

As in the preceding studies,[1−4] we used the RDX Buckingham potential plus Coulombic interactions terms obtained through fitting of partial charges centered on each atom in the experimental arrangement of the molecule to a quantum mechanically derived electrostatic potential.[7] Moreover, as in the case of the nitramine crystals,[4] we have investigated how the geometrical and energetic parameters predicted in molecular packing calculations depend on charges calculated from ab initio methods that do or do not include electron correlation effects. Specifically, we used different sets of charges derived from the Hartree−Fock (HF) wave function[8] or from methods that employ electron correlations such as second-order Möller−Plesset (MP2)[9] and density functional theory (DFT).[10] We again note that the main limitation of the calculations is the assumption of rigid molecules, but this model can be used to study processes at temperatures and pressures where molecular deformations are negligible. Our intent is to extend the model to allow for deformation of the molecules by incorporating intramolecular interaction terms.

The organization of the paper is as follows. In section II, the intermolecular potential used to simulate the crystals is presented. In sections III, the details of calculations using molecular packing methods and isothermal−isobaric MD calculations are described. The results of these calculations are given in section IV. The main conclusions are summarized in section V.

II. Intermolecular Potential

In this work, we adopt the same general principles for atom−atom potentials that proved to be successful in modeling of the nitramine crystals.[1−4] In particular, we assume that (a) the intermolecular interactions depend only on the interatomic distances, (b) the interaction potential can be separated into contributions identified as van der Waals and electrostatic, and (c) the same type of van der Waals potential is used for the same type of atoms, independent of their state of valence. Moreover, we assume the transferability of the potential parameters between similar molecules; that is, we extend the validity of the potential parameters determined for RDX crystal to all the nitro compounds considered in the present database.

We approximate the intermolecular interactions between the molecules of the crystal as a pairwise sum of Buckingham (6-exp) (repulsion and dispersion) and Coulombic (C) potentials of the form

$$V_{\alpha\beta}^{6-\exp}(r) = A_{\alpha\beta}\exp(-B_{\alpha\beta}r) - C_{\alpha\beta}/r^6 \qquad (1)$$

and

$$V_{\alpha\beta}^{C}(r) = \frac{q_\alpha q_\beta}{4\pi\epsilon_0 r} \qquad (2)$$

where r is the interatomic distance between atoms α and β, q_α and q_β are the electrostatic charges on the atoms, and ϵ_0 is the dielectric permittivity constant of vacuum.

The parameters for the 6-exp potential in eq 1 are those previously determined for the RDX crystal.[1] We use the same combination rules for calculating the heteroatom parameters from homoatom parameters as previously reported.[1] The assignments of the electrostatic charges were made by fitting a set of atom-centered monopole charges for the isolated molecule to reproduce the quantum mechanically derived electrostatic potential, which is calculated over grid points surrounding the van der Waals surface of the molecules. This method of fitting the electrostatic potential was proposed by Breneman and Wiberg[7] and is incorporated in the Gaussian 94 package of programs[11] under the keyword CHELPG (electrostatic-potential-derived atomic charges). The quantum mechanical calculations have been done at the Hartree−Fock (HF),[8] second-order

Möller−Plesset (MP2),[9] and density functional theory (DFT)[10] levels to investigate the effect of electron correlation. The density functional that was used includes the exchange functional described by the fitted three-parameter hybrid of Becke[12] and the correlation functional of Lee, Yang, and Parr (Becke3-LYP).[13] All of the above theoretical calculations were done using the basis set 6-31G** (split-valence plus d-type and p-type polarization functions).[14]

It has been previously shown[15,16] that the neglect of electron correlation in self-consistent wave functions results in an overestimation of the electrostatic interactions and that this overestimate is mainly a scaling effect. A scaling factor of 0.9 was shown to give improved agreement between the calculated and the experimental dipole moments for a set of eight small molecules,[15] in a study of the electrostatic interactions of a dipeptide,[16] and in determining the crystal structures of polar organic molecules.[17] Our previous study of the nitramine crystals[4] showed that the use of the 0.9 scaling factor for the electrostatic charges determined at the HF level significantly improves the accuracy of the predicted lattice energies of the crystals. We further investigate in the present study different electrostatic models and evaluate the effects of the scaling procedure. Specifically, four electrostatic models were tested for each of the 51 crystals. Two of them use electron correlation methods, namely MP2 and B3LYP, the third one uses unscaled HF charges, and the last employs the HF charges scaled by 0.9 (denoted as 0.9HF).

III. Computational Approach

Molecular Packing Calculations. Molecular packing calculations are used to test empirical or semiempirical intermolecular potential energy functions of organic crystals.[18,19] The calculations minimize the lattice energy of the models with respect to the structural degrees of freedom in the crystals. For crystals in which the asymmetric unit contains one molecule that occupies an arbitrary position, the maximum number of degrees of freedom is 12. These correspond to the six unit cell constants (a, b, c, α, β, γ), the three rotations (θ_1, θ_2, θ_3), and the three translations (τ_1, τ_2, τ_3) of the rigid molecule. The number of structural degrees of freedom might be reduced depending on the symmetry restrictions of the space group. Crystals in which the asymmetric unit contains more than one molecule have additional degrees of freedom to describe the rotation and translation of the molecules. As in the case of nitramine crystals,[4] we consider that the crystals can be represented as an ensemble of rigid molecules.

A stable crystal configuration is obtained by assuming that the crystal energy can be represented as a function of the structural lattice parameters and minimizing the crystal energy with respect to the structural lattice parameters. The minimization is performed using traditional steepest-descent and Newton−Raphson procedures.[20,21]

Two series of MP calculations were performed. In the first series, the energy minimizations were performed for all the crystals using the program PCK91.[22] Starting configurations correspond to the experimentally observed geometries. This program employs the accelerated convergence method[1,20] for accurate evaluation of the crystal Coulombic and dispersion lattice sums, with the first and second derivatives of the crystal energy evaluated analytically. The space group symmetry is maintained throughout the energy minimization, reducing the number of independent variables in the minimization procedure. For example, nitromethane (see entry 1 in Table 1S of the Supporting Information) has space group symmetry $P2_12_12_1$ ($Z = 4$). In this case, the crystallographic parameters varied in the minimization using the PCK91 program are the three dimensions of the unit cell and the three rotations and translations of the molecule in the asymmetric unit cell. The three angles α, β, and γ of the unit cell were set at 90° and were not allowed to vary. The structural shift factor [21,23]

$$F = (\Delta\theta/2)^2 + (10\Delta x)^2 + (100\Delta a/a)^2 + (100\Delta b/b)^2 + (100\Delta c/c)^2 + (\Delta\alpha)^2 + (\Delta\beta)^2 + (\Delta\gamma)^2 \quad (3)$$

provides a measure of the quality of the predicted geometrical crystallographic parameters relative to the experimental values; $\Delta\theta$ is the total root-mean-square (rms) rigid-body rotational displacement (in degrees) after minimization, Δx is the rms total rigid-body translational displacement (in angstroms), a, b, c, α, β, and γ are the cell-edge lengths and angles of the unit cell, respectively.

We have previously shown[1,2,24] that, when an accurate intermolecular potential is used, the removal of the symmetry constraints in MP calculations has only a very small effect on the final lattice energies and crystallographic parameters. Moreover, the crystal symmetry, analyzed at the beginning and at the end of the energy minimization, remained unchanged. In the present work, we have tested the effect of removing the imposed symmetry constraints in a second series of MP calculations for 17 of the 51 crystals. These calculations have been done using the algorithm proposed by Gibson and Scheraga[25] for efficient minimization of the energy of a fully variable lattice composed of rigid molecules and implemented in the program LMIN.[26] In these calculations, the parameters P and Q, which specify the start and the end of the cubic feather (see refs 1 and 25 for details), were set to 20.5 and 20.0, respectively.

As in our earlier studies, we analyzed the crystal symmetry of each of the 17 systems at the beginning and the end of the energy minimization to determine if the crystal space group was conserved in the energy minimization. The space group is considered to be conserved if the symmetry operations, as defined in the International Tables of Crystallography,[27] between the molecule(s) in the asymmetric unit cell and the remaining molecule(s) in the unit cell are unchanged and if the lattice parameters fixed by the lattice symmetry have not been modified significantly.

Another quantity of interest is the lattice energy of crystals. When different crystallographic phases exist, the lattice energy can provide information about their relative stabilities. Moreover, the calculated static lattice energy of the crystals can be compared to the experimental sublimation enthalpy based on the relation[28] $-\Delta H_{\mathrm{subl}} = E + K_0 + 2RT$, where E is the lattice energy and K_0 is the zero-point energy. Often, a rough estimate of the lattice energy is obtained by neglecting the K_0 term. Kitaigorodski[18] has pointed out that considering the inaccuracy involved in the experimental determination of ΔH_{subl} and due to neglect of zero-point energy, discrepancies up to 3−4 kcal/mol between the calculated and the observed enthalpies of sublimation are expected.

Isothermal−Isobaric Molecular Dynamics Calculations. A more stringent test of the intermolecular interaction potential is accomplished through prediction of the structural lattice parameters by isothermal−isobaric MD simulations at different temperatures. We have performed such calculations for two of the most important energetic crystals in our database, namely the monoclinic phase of 2,4,6-trinitrotoluene (TNT) (entry 14, Table 1S of the Supporting Information) and the tetragonal phase

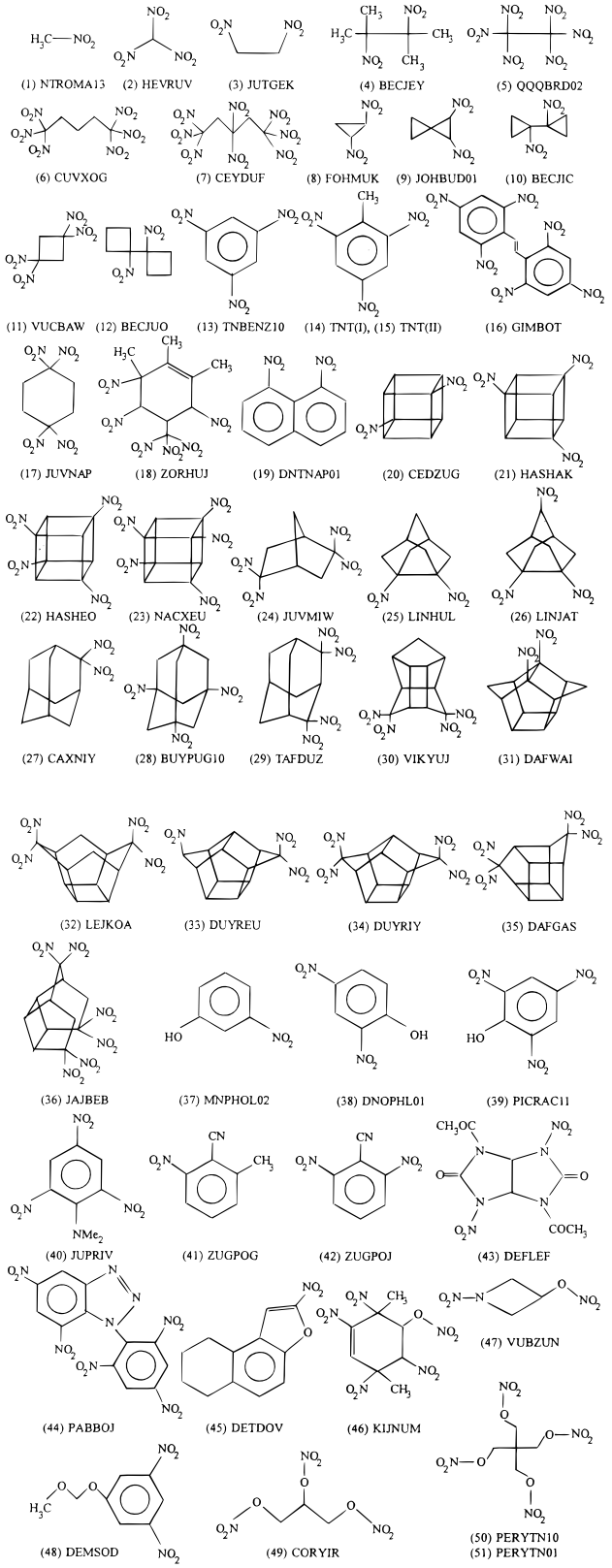

Figure 1. Illustration of the molecules whose crystal structures were studied. Where available, the corresponding refcode entry in the Cambridge Structural Database[33] is indicated.

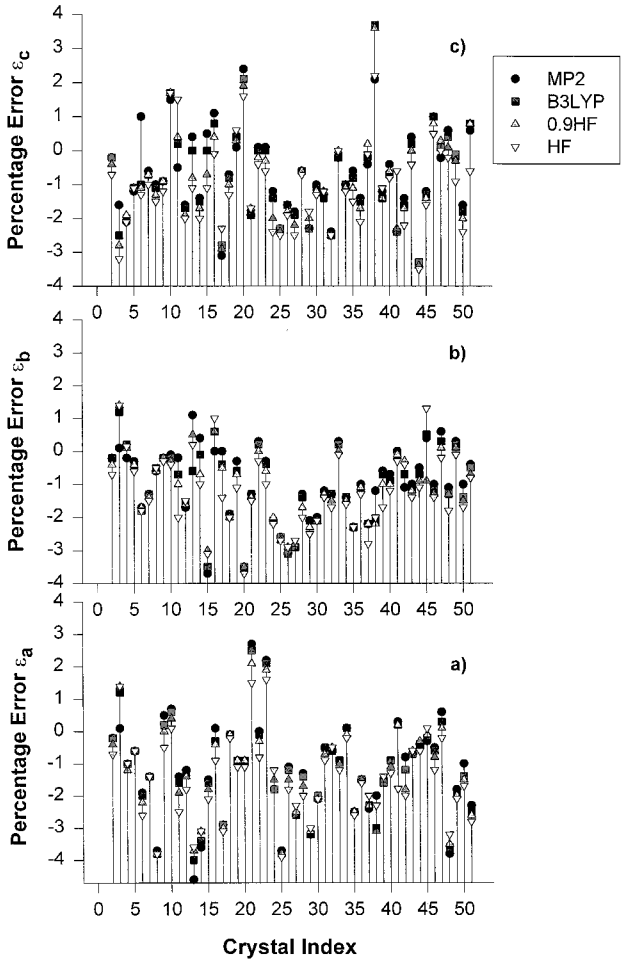

Figure 2. Calculated percentage errors between the predicted and the experimental values of the lattice dimensions a in (a), *b* in (b) and *c* in (c) for all crystals given in Table 1S of the Supporting Information. The crystal index corresponds to the order number in Table 1S.

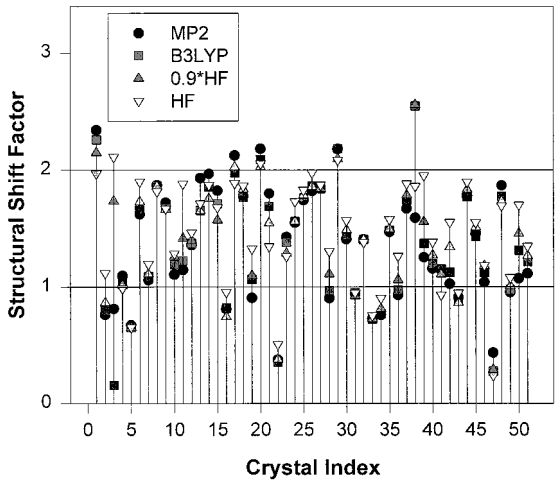

Figure 3. Calculated structural shift factor *F* (eq 3) for the crystal structures in the database as a function of the electrostatic set of charges. The crystal index corresponds to the order number in Table 1S of the Supporting Information. The horizontal lines at 1% and 2% are marked for a more clear view of the distribution of points.

of pentaerythritol tetranitrate (PETN I) (entry 50, Table 1S). Simulations were performed at atmospheric pressure and temperatures from 100 to 350 K for TNT and 100−400 K for PETN using the algorithm proposed by Nosé and Klein[29] as implemented in the program MDCSPC4B.[30] Since details of the calculations are given in ref 1, we will give only a brief description of the computational parameters. The MD simulation cells consist of boxes containing 16 ($2 \times 4 \times 2$) and 36 ($3 \times 3 \times 4$) unit cells for TNT and PETN I, respectively. The lattice sums were calculated subject to minimum-image periodic boundary conditions in all dimensions.[31] The interactions were

TABLE 1: Comparison of the Experimental and Calculated Lattice Energies for Different Sets of Electrostatic Charges Using Molecular Packing with Symmetry Constraints

		lattice energy (kJ/mol)				
	crystal	HF/6-31G**	0.9 HF/6-31G**	B3LYP/6-31G**	MP2/6-31G**	ΔH_{sub} (kJ/mol)*
1.	NTROMA13	−60.10	−53.50	−50.83	−49.38	
2.	HEVRUV	−80.84	−74.67	−71.34	−70.20	54.8 ± 4.2[36a]
3.	JUTGEK	−104.16	−93.40	−87.42	−85.31	
4.	BECJEY	−121.86	−112.41	−107.53	−106.08	
5.	QQQBRD02	−103.18	−102.11	−101.77	−101.56	70.7 ± 1.7[36b]
6.	CUVXOG	−181.68	−177.88	−171.51	−168.89	
7.	CEYDUF	−161.05	−155.43	−152.74	−151.49	
8.	FOHMUK	−96.24	−88.38	−84.49	−81.68	
9.	JOHBUD01	−112.26	−104.03	−101.07	−98.72	
10.	BECJIC	−110.73	−103.17	−99.47	−96.17	
11.	VUCBAW	−140.86	−129.99	−124.19	−121.46	
12.	BECJUO	−121.83	−114.52	−110.01	−107.42	
13.	TNBENZ10	−132.55	−123.69	−118.11	−114.48	107.3 ± 0.6[36c]
14.	TNT-phase I	−151.98	−141.49	−135.57	−130.97	118.4 ± 4.2[36d]
15.	TNT-phase II	−149.40	−139.28	−133.16	−128.70	
16.	GIMBOT	−257.38	−238.13	−225.41	−216.36	179.9[36d]
17.	JUVNAP	−164.15	−152.72	−146.14	−143.04	
18.	ZORHUJ	−177.78	−167.66	−160.68	−157.57	
19.	DNTNAP01	−139.38	−131.59	−126.66	−123.25	
20.	CEDZUG	−141.29	−131.55	−128.17	−124.99	
21.	HASHAK	−161.73	−148.04	−142.26	−138.04	
22.	HASHEO	−190.42	−172.25	−163.13	−158.31	
23.	NACXEU	−206.61	−187.59	−177.10	−171.47	
24.	JUVMIW	−157.15	−146.64	−141.04	−137.90	
25.	LINHUL	−138.27	−130.74	−127.00	−123.95	
26.	LINJAT	−161.74	−150.76	−144.70	−141.01	
27.	CAXNIY	−122.41	−119.31	−117.17	−115.95	96.4 ± 1.4[36e]
28.	BUYPUG10	−188.16	−173.58	−164.72	−160.95	
29.	TAFDUZ	−155.25	−149.45	−145.27	−143.42	
30.	VIKYUJ	−169.39	−161.57	−156.96	−154.25	
31.	DAFWAI	−151.70	−145.12	−141.75	−139.03	
32.	LEJKOA	−178.37	−169.02	−162.62	−159.09	
33.	DUYREU	−162.77	−155.44	−151.10	−148.62	
34.	DUYRIY	−173.64	−164.69	−159.68	−156.96	
35.	DAFGAS	−168.90	−159.12	−153.77	−151.05	
36.	JAJBEB	−200.03	−187.13	−180.24	−176.83	
37.	MNPHOL02	−101.37	−95.34	−94.96	−93.61	91.6 ± 2.1[36a,f]
38.	DNOPHL01	−120.42	−112.81	−110.41	−107.39	104.6 ± 4.2[36g]
39.	PICRAC11	−152.55	−141.58	−135.30	−129.16	105.1 ± 1.6[36c]
40.	JUPRIV	−148.23	−140.90	−138.97	−135.27	
41.	ZUGPOG	−119.24	−111.60	−110.41	−108.05	
42.	ZUGPOJ	−140.83	−130.12	−126.87	−124.04	
43.	DEFLEF	−214.53	−195.65	−187.30	−179.94	
44.	PABBOJ	−113.31	−106.49	−103.22	−101.21	
44.	PABBOJ	−226.63	−212.98	−206.47	−202.42	
45.	DETDOV	−129.86	−127.15	−126.94	−124.59	
46.	KIJNUM	−176.93	−162.62	−153.67	−149.16	
47.	VUBZUN	−114.56	−104.71	−102.95	−100.50	
48.	DEMSOD	−143.62	−135.33	−133.15	−130.60	
49.	CORYIR	−147.60	−136.87	−132.70	−131.54	
50.	PERYTN10	−221.09	−202.46	−193.77	−170.38	
51.	PERYTN01	−178.65	−166.87	−161.77	−156.84	151.9± 2.1[36a,h]

[a] The corresponding references are given in ref 36.

determined between the sites (atoms) in the simulation box and the nearest-image sites within the cutoff distance. Cutoff distances were set at 11.0 Å for both crystals. In the initial simulation corresponding to the lowest temperature, the position and orientation of the molecules in the unit cell were taken to be those for the experimental structure. The initial velocities of the centers of mass of the molecules were selected at random, but were modified to eliminate the translation and rotation of the bulk MD cell. The trajectories were integrated for 12 000 time steps (1 time step $= 2 \times 10^{-15}$ s), of which 2000 steps were equilibration. In the equilibration period, the velocities were scaled after every five steps such that the internal temperature of the crystal mimics the imposed external temperature. Then, average properties were calculated over the remaining integration steps in the simulation. In subsequent runs, performed at successively higher temperatures, the initial configurations of the molecular positions and velocities were taken from the previous simulation at the end of the production run. The velocities were again scaled over an equilibration period of 2000 steps, to achieve the desired external temperature, followed by a 10 000-step production run.

Several types of quantities were determined to obtain information about structural parameters of the crystal. These include the mean lattice geometrical parameters, the cumulative mass-center radial distribution functions (RDF), and the average positions and orientations of the molecules. These quantities were obtained from values calculated at every 10th step during the trajectory integrations.

TABLE 2: Lattice Parameters and Energies Obtained in Crystal-Packing Calculations without Symmetry Constraints[a]

	final lattice parameters						
crystal	*a* (Å)	*b* (Å)	*c* (Å)	α (deg)	*β* (deg)	*γ* (deg)	final energy
HEVRUV	10.3411 (−0.1)	10.3412 (−0.1)	10.3422 (−0.1)	89.99 (0.0)	89.99 (0.0)	89.99 (0.0)	−70.22
BECJEY	6.2379 (−1.0)	6.2898 (0.2)	11.6008 (−2.1)	100.02 (−0.7)	80.26 (−0.9)	118.21 (−0.4)	−106.11
TNBENZ10	9.3251 (−4.6)	27.2363 (1.1)	12.8791 (0.4)	89.99 (0.0)	89.99 (0.0)	89.98 (0.0)	−114.46
TNT I	20.5078 (−3.6)	6.1176 (0.4)	14.8125 (−1.4)	90.00 (0.0)	110.39 (0.2)	89.99 (0.0)	−131.02
TNT II	14.7733 (−1.5)	19.2835 (−3.7)	6.1343 (0.6)	89.99 (0.0)	89.99 (0.0)	90.00 (0.0)	−128.97
GIMBOT	22.3504 (0.1)	5.5723 (0.0)	14.8260 (1.0)	90.00 (0.0)	111.13 (0.9)	89.99 (0.0)	−216.47
NACXEU	6.7829 (2.2)	23.2037 (−0.3)	7.8659 (0.1)	90.00 (0.0)	114.89 (1.5)	89.99 (0.0)	−171.46
JUVMIW	8.4259 (−1.8)	10.4800 (−2.0)	11.5478 (−1.2)	90.00 (0.0)	90.00 (0.0)	89.99 (0.0)	−137.94
LINHUL	6.4673 (−3.7)	11.9504 (−2.6)	12.9740 (−2.2)	63.90 (−0.3)	81.62 (−0.2)	88.69 (−0.6)	−123.98
BUYPUG10	7.7691 (−1.3)	7.7692 (−1.3)	10.4845 (−0.64)	89.99 (0.0)	90.00 (0.0)	89.99 (0.0)	−161.00
DUYRIY	9.5770 (0.1)	11.5415 (−1.4)	11.7313 (−1.0)	76.60 (−0.2)	89.66 (0.3)	88.27 (0.1)	−156.89
PICRAC11	9.1385 (−1.3)	19.0092 (−0.6)	9.5956 (−1.2)	90.00 (0.0)	90.00 (0.0)	89.99 (0.0)	−257.50
JUPRIV	8.2936 (−0.9)	16.3874 (−0.7)	8.6169 (−0.4)	90.01 (0.0)	199.58 (1.5)	89.99 (0.0)	−133.18
DEFLEF	6.8144 (−0.6)	9.5411 (−1.0)	18.6262 (0.4)	90.00 (0.0)	90.00 (0.0)	89.99 (0.0)	−180.03
PABBOJ	6.6714 (−0.4)	20.2231 (−0.5)	11.4702 (−3.3)	89.99 (0.0)	90.00 (0.0)	90.00 (0.0)	−201.87
PETNI	9.2832 (−1.0)	9.2841 (−1.0)	6.5995 (−1.6)	90.00 (0.0)	90.00 (0.0)	90.00 (0.0)	−170.51
PETNII	12.9845 (−2.3)	13.4333 (−0.4)	6.8734 (0.6)	90.00 (0.0)	90.00 (0.0)	90.00 (0.0)	−156.88

[a] The values in parentheses are the percent difference relative to experimental values.

TABLE 3: Predicted Lattice and Volume Parameters as Functions of Temperature. The Calculated Thermal Expansion Coefficients (*χ*) at 300 K Are Also Indicated.

T (K)	*a* (Å)	*b* (Å)	*c* (Å)	α (deg)	*β* (deg)	*γ* (deg)	volume (Å^3)
			TNT I				
exptl[a]	21.2750	6.09301	5.0250	90.0	110.14	90.0	1828.57
100.0	20.5812	6.13851	4.8520	90.00	110.37	89.99	1758.71
200.0	20.6753	6.16141	4.8971	89.98	110.33	90.02	1779.16
273.1	20.7553	6.18001	4.9299	90.01	110.34	89.99	1795.19
300.0	20.7839	6.18751	4.9452	89.97	110.31	90.02	1802.03
350.0	20.8418	6.20111	4.9742	89.99	110.31	90.00	1814.50
χ[b]	54.0×10^{-6}	43.4×10^{-6}	34.6×10^{-6}				135.8×10^{-6}
			PETN I				
exptl	9.3776	9.3776	6.7075	90.0	90.0	90.0	589.85
100.0	9.3039	9.3094	6.6164	90.00	89.99	89.99	572.97
200.0	9.3218	9.3254	6.6327	89.98	89.86	89.99	576.48
273.1	9.3399	9.3387	6.6491	89.98	89.98	89.99	579.91
300.0	9.3472	9.3470	6.6571	89.99	89.98	90.00	581.50
350.0	9.3576	9.3550	6.6686	90.01	90.00	89.99	583.56
400.0	9.3680	9.3720	6.6756	89.99	90.00	89.99	585.98
χ	22.7×10^{-6}	21.2×10^{-6}	31.0×10^{-6}				75.7×10^{-6}

[a] The experimental values at 300 K. [b] The units for the liniar and volume expansion coefficients are K^{-1}.

IV. Results and Discussions

Molecular Packing Calculations with Symmetry Constraints. The 51 nitro compounds considered in this study are shown in Figure 1. This set of crystals includes nitroalkanes, nitroaromatics, nitrocubanes, polynitroadamantanes, polynitropolycycloundecanes, polynitropolycyclododecanes, hydroxynitro derivatives, nitrobenzonitriles, nitrobenzotriazoles, and nitrate esters. Our selection includes some important examples of energetic crystals such as TNT, PETN, and polynitro cage compounds. The structures of most of these crystals have been determined by X-ray diffraction techniques. Despite the generally poorer resolution of hydrogen atom positions obtained by these techniques, we have not done any additional adjustments of these positions to give, for example, the standard bond lengths.[32] The crystal structures in Figure 1 are denoted by the corresponding crystal "refcode" used in the Cambridge Structural Database.[33] The corresponding names of the molecules are given in ref 34 and assigned a crystal index number, which are used to reference individual molecules in the figures and tables presented here. The structures used for monoclinic and orthorhombic forms of TNT were taken from the unpublished work of J. R. C. Duke [ref 35 (15)] so they do not have a refcode. In addition, we have studied different crystallographic phases of the TNT and PETN crystals. The specific references for all 51 crystals are given in ref 35.

The results of MP calculations using the PCK91 program are presented in supplemental Table 1S. The results in this table and Figure 2 show that the predicted structural lattice parameters for almost all of the crystals differ by less than 3% from the experimental structures. The largest differences are for the TNBENZ10 (entry 13, Table 1S of the Supporting Information) crystal with a maximum value of −4.6% for one of the lattice dimensions. However, this decreases to −3.6% when the HF set of charges is used. In addition, for the majority of the crystals, there are small rotations and practically no translations for the molecules in the asymmetric unit cell. The overall accuracy of the predicted models is evident in Figure 3, which shows the structural drift factors described in eq 3. For the majority (69%) of crystals, the structural shift factor is between 1 and 2, while in 23% of the cases this factor is less than 1.0.

Table 1S of the Supporting Information and Figure 3 show the influence of the set of electrostatic charges calculated at different ab initio levels. It is found that in 9 of the 51 crystals the structural shift factor increased when the HF set of charges was replaced with the MP2 set. In a number of instances (see, e.g., entries 5, 8, and 31), there is no significant variation of the shift factors with the set of electrostatic charges employed.

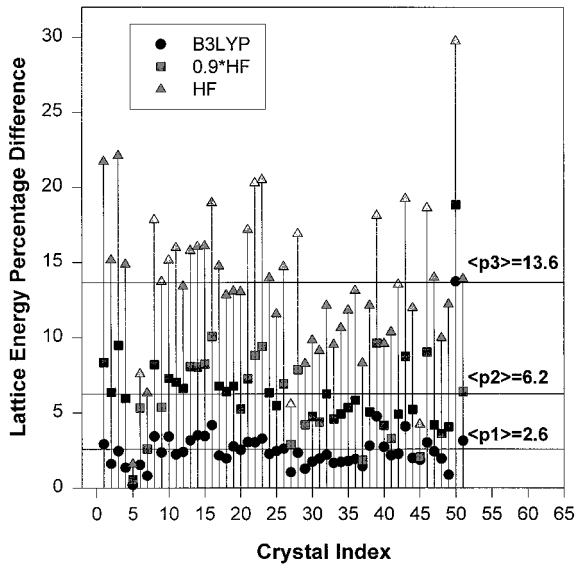

Figure 4. Calculated lattice energies in percentage difference relative to the corresponding MP2 values. The crystal index corresponds to the order number in Table 1S of the Supporting Information. The three horizontal lines indicate the average deviations for the energies calculated using the B3LYP ($\langle p1 \rangle = 2.6\%$), 0.9*HF ($\langle p2 \rangle = 6.2\%$) and HF ($\langle p3 \rangle = 13.6\%$) sets of charges.

However, for most crystals, the use of B3LYP and MP2 charges improves the agreement between the predicted and the experimental lattice parameters. Some large improvements can be seen, for example, in the cases of JUTGEK and VUCBAW (entries 3 and 11 of Table 1S, respectively), where the relative errors from the experimental lattice parameters decrease by more than 1% for some lattice dimensions. However, in almost all cases, the variations of the geometrical lattice dimensions are less than 1% with respect to the change of the set of electrostatic charges.

We can also see from the results in Table 1S and Figure 3 that when the electrostatic charges calculated at the HF level are scaled by 0.9, the predicted geometrical parameters are very close to those obtained at the MP2 level. Moreover, the structural shift factors appear generally to have values intermediate between the MP2 and HF values.

The lattice energies predicted by different models are given in Table 1S of the Supporting Information. As can be seen by comparing the data for MP2, B3LYP, and HF methods, the use of the correlated methods determines the decrease of the absolute lattice energy. This effect can be understood as a consequence of the decrease in the absolute value of the electrostatic interaction, which has a predominant attractive character. The variations in the absolute values of the HF lattice energies are between 1.6% and 30% relative to the lattice energies determined at MP2 level, with an average difference of 13.6% (see Figure 4). The use of the 0.9 scaling factor reduces these differences in the range 0.5−19% with an average difference of 6.2%. Finally, the B3LYP lattice energies are, as expected, much closer to the MP2 energies, with a range of variation between 0.2 and 13.7% and with an average difference of 2.6%. These results indicate that the lattice energies differ significantly for sets of electrostatic charges calculated with ab initio methods that do or do not include the electron correlation. These differences can be decreased by a factor of ∼2 when the HF charges are scaled. Another important result is that DFT methods can provide charges that give a similar accuracy (within 2.6%) for the lattice energy to that determined at the MP2 level. This finding is notable since the computational time necessary for B3LYP is significantly lower than that for MP2. The corresponding average differences we have found in the case of nitramine crystals[4] were equal to 12.8%, 4.1%, and 2.6%, respectively, for the HF, 0.9HF, and B3LYP set of charges. The coincidence of the results found at the B3LYP level is an indication that, in both the previous and present work, the B3LYP charges represent a good approximation and a viable alternative to the more computer time demanding MP2 charges.

In Table 1 we compare the calculated lattice energies to the available experimental sublimation enthalpies. Despite the limited number of experimental values given in Table 1, it can be seen that a significant improvement in the accuracy of the predicted lattice energies can be obtained by using the electrostatic charges determined by methods that treat electron correlation. The scaling of the HF charges also leads to improvements in the predicted energies, but the differences from the experimental values are larger than those obtained when the charges are calculated with electron correlation methods. In absolute values, the MP2 energies for the majority of crystals are within the acceptance range of 12−17 kJ/mol of the experimental lattice energies, as previously recommended by Kitaigorodsky.[18] Exceptions are the QQBRD02 and GIMBOT crystals where the differences are larger. However, the lack of agreement between the calculated and experimental lattice energies does not correlate with the accuracy of the predicted geometrical parameters. In particular, for these two crystals, the predicted lattice parameters are quite good (see entries 5 and 16 in Table 1S) with maximum structural shift factors of 0.675 and 0.955, respectively.

We have also determined the relative stability of some crystals that have different phases. Specifically, we focused on the relative stabilities of the polymorphic phases of TNT and PETN crystals. In the TNT case, the calculated MP2 lattice energies for the monoclinic and orthorhombic phases are −130.97 and −128.70 kJ/mol, respectively. These values indicate that the monoclinic phase is more stable than the orthorhombic phase, in agreement with experimental findings.[37] Moreover, the difference between the predicted lattice energies of these two polymorphs, 2.3 kJ/mol, represents the energy of transformation from the monoclinic to the orthorhombic phases. This result compares well with the experimental value $\Delta H_{tr} = 1.13$ kJ/mol.[38] In the case of PETN crystal, our intermolecular potential predicts that the tetragonal phase (PERYTN10) is more stable than the orthorhombic phase (PERYTN01), also in agreement with the experimentally determined stability ranking.[39]

Molecular Packing Calculations without Symmetry Constraints. The results of molecular packing calculations for the set of 17 crystals arbitrarily chosen from the entire set are given in Table 2. These calculations were done using the MP2 charges only. As can be seen by comparing the data in Table 2 with that in Table 1S of the Supporting Information, there is very good agreement between the geometric and energetic values predicted in molecular packing with and without symmetry constraints. Small differences in the total lattice energies (<0.5 kJ/mol) between the constrained and unconstrained calculations are due to differences in the evaluation of the dispersion lattice sums. The unconstrained simulations do not use the accelerated convergence method for this evaluation. In addition, we have verified that the symmetry operations at the beginning and at the end of energy minimization are unchanged. This indicates that the interaction potential sufficiently describes the known crystallographic symmetries of these crystals.

NPT Molecular Dynamics Calculations. NPT-MD calculations have been performed for the most stable crystal phases of TNT (monoclinic) and PETN (tetragonal, denoted PETN I).

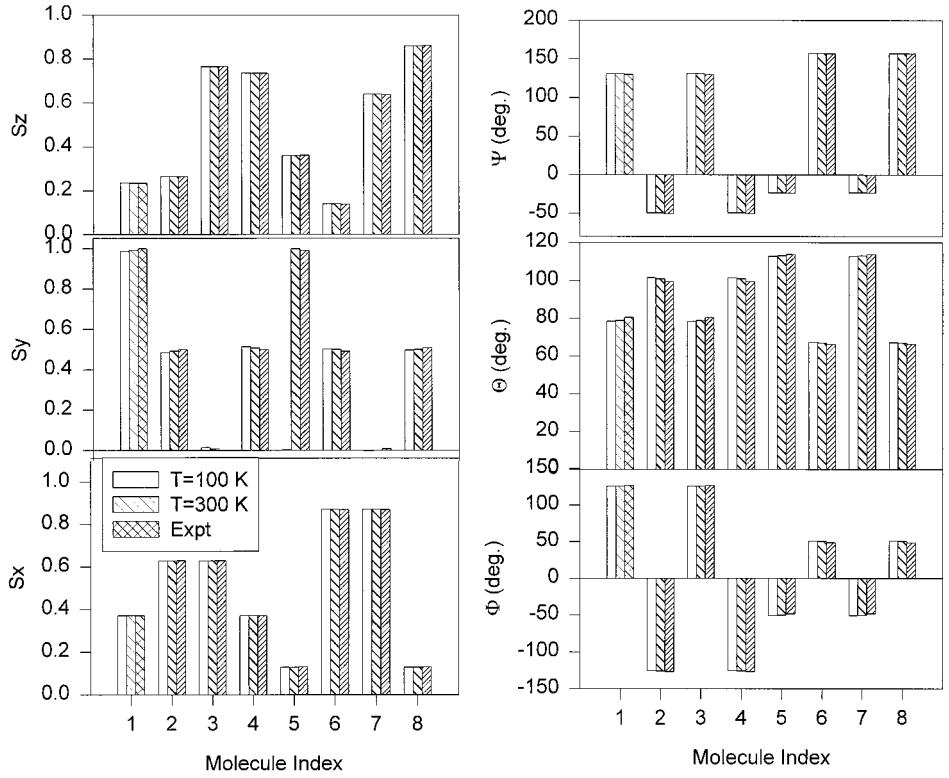

Figure 5. Comparison of the average fractional coordinates and Euler angles of the eight molecules in the unit cell of TNT (monoclinic phase) with the corresponding experimental values.

These calculations used the set of MP2 charges only. The crystal structure information resulting from NPT-MD simulations at atmospheric pressure and different temperatures is given in Table 3. In both TNT and PETN I, the lattice dimensions obtained at $T = 100$ K (Table 3) are in very good agreement with those determined from the MP calculations with symmetry constraints (Table 1S of the Supporting Information). This is expected, since the thermal effects at 100 K should be minimal and the thermal averages at this temperature should be close to the values corresponding to the potential energy minimum. At 300 K, the average lattice dimensions of these crystals agree very well with the experimental values; the corresponding differences for the *a*, *b*, and *c* lattice dimensions are 2.30%, 1.55%, and 0.53% for TNT and 0.32%, 0.32%, and 0.75% for PETN I, respectively. In addition, in both cases the angles of the unit cell are close to the experimental values. At 300 K, the difference between the calculated and the experimental volume of the unit cell is 1.45% for TNT and 1.41% for PETN I.

Figure 5 provides a visual comparison of the average mass-center fractionals and Euler angles for each of the eight molecules within the unit cell of TNT with experimental values. Increasing the temperature from 100 to 300 K does not produce any significant displacement of the molecular mass-centers or increase the degree of rotational disorder. Similar conclusions about the degrees of translational and rotational disorder were obtained in the case of PETN I (not shown).

Additional evidence for the small degree of translation of the molecules inside the unit cell with increasing temperature can be obtained from the mass-center−mass-center radial distribution functions (RDFs). These are given in Figure 6. The RDFs for both crystals exhibit well-ordered structure, with correlations at long distances even at the higher temperatures. The positions of the major peaks do not change significantly, and the main temperature effects are the broadening of the peaks and the partial overlapping of some of them. For example, in

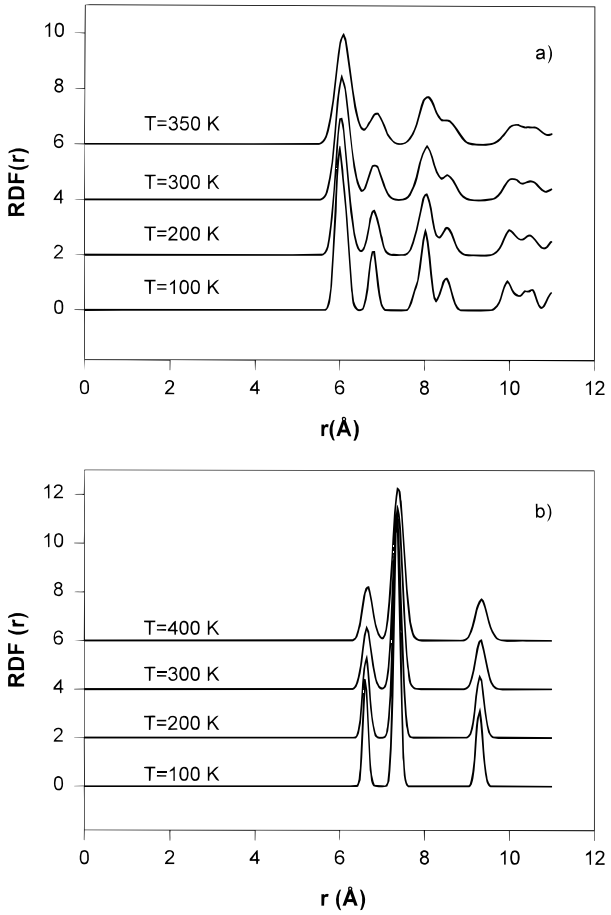

Figure 6. Variation of the center of mass−center of mass radial distribution function as a function of temperature for TNT (a) and PETN (b).

the case of PETN I, the centers of mass of the two molecules in the unit cell occupy the special fractional positions (0,0,0) and (1/2,1/2,1/2). There are only three specific distances between these positions and they correspond to very distinct peaks in the RDF spectrum (see Figure 6b).

We have also determined the linear and volume expansion coefficients at 300 K for these crystals using the temperature dependence of the lattice dimensions. The values for these quantities are given in Table 3. For TNT, the values of 5.0×10^{-5} K^{-1} and 18.0×10^{-5} K^{-1} have been determined for the linear and volume expansion coefficients in the temperature range 291−318 K.[40] The measured linear expansion coefficients are in relatively good agreement with the values predicted by our potential. Also, our calculated volume expansion coefficient is about 28% smaller than the reported experimental value.

In the case of PETN I, the values of 7.65×10^{-5} K^{-1} and 23.2×10^{-5} K^{-1} have been reported for the linear and volume expansion coefficients.[41] These values are a factor of 3 larger than our calculated expansion coefficients. Although the interaction potential can reasonably predict the individual lattice dimensions and volume at room temperature, these differences suggest that it does not adequately describe the magnitude of the thermal expansion. However, the thermal expansion coefficients along the *a* and *b* axes are quite similar, in agreement with the tetragonal symmetry of this crystal.

V. Conclusions

We have investigated the degree of transferability of a 6-exp Buckingham potential previously parametrized using experimental information for the α-RDX crystal[1] to 51 non-nitramine crystals, consisting of different types of nitroalkanes, nitroaromatics, nitrocubanes, polynitroadamantanes, polynitropolycycloundecanes, polynitropolycyclododecanes, hydroxynitro derivatives, nitrobenzonitriles, nitrobenzotriazoles, and nitrate esters. The intermolecular potential includes Coulombic interactions between electrostatic charges. These charges have been determined from fits to ab initio electrostatic potentials calculated for the individual molecules in the experimental configurations. We have considered four different electrostatic models, with charges determined at HF, B3LYP, and MP2 levels and at the HF level uniformly scaled by a factor of 0.9.

The tests of this potential for the entire collection of 51 crystals have been performed using MP calculations with symmetry constraints. For a smaller set of crystals, we have verified that MP packing without symmetry constraints predicts essentially the same lattice dimensions and energies. The predicted crystal structural parameters are in good agreement with the experimental values for most of the crystals, with differences generally less than 3%. For 92% of the crystals in the collection, the structural shift factor is less than 2.0.

There is only a small influence (generally less than 1%) on the crystallographic parameters by the set of electrostatic charges used. However, the lattice energies of the crystals are significantly influenced by the electrostatic model. In particular, the best agreement with the experimental lattice energies has been obtained for the MP2 charges. The lattice energies calculated using the B3LYP charges overestimate the MP2 energies by about 2.6%, while the HF charges overestimate the MP2 energies by 13.6%. The procedure of uniformly scaling the HF charges by the 0.9 factor decreases the differences to about 6.2%.

In the case of the TNT and PETN I crystals, the intermolecular potential describes the correct order of stability of different phases. The predicted stabilities monoclinic > orthorhombic in TNT and tetragonal > orthorhombic in PETN are in accord with experimental findings.[37,39]

Moreover, the results of NPT-MD simulations for ambient conditions of temperature and pressure support the good agreement of the predicted and experimental crystallographic values.

The success of the present potential energy parameters in describing different types of crystals containing molecules with functional groups associated with explosives provides significant incentive to further develop this model through the incorporation of the intramolecular degrees of freedom. This will be done in future work.

Acknowledgment. This work was supported by the Strategic Environmental Research and Development Program (SERDP), Project PP-695. D.L.T. gratefully acknowledges support by the U. S. Army Research Office under Grant DAAG55-98-1-0089.

Supporting Information Available: A table (Table 1S) giving a comparison of the crystallographic parameters determined by molecular packing calculations and experimental values for all molecular structures considered in this paper. This material is available free of charge in the Internet at http://pubs.acs.org.

References and Notes

(1) Sorescu, D. C.; Rice, B. M.; Thompson, D. L. *J. Phys. Chem*. B **1997**, *101*, 798.

(2) Sorescu, D. C.; Rice, B. M.; Thompson, D. L. *J. Phys. Chem. B* **1998**, *102*, 948.

(3) Sorescu, D. C.; Rice, B. M.; Thompson, D. L. *J. Phys. Chem.*, in press.

(4) Sorescu, D. C.; Rice, B. M.; Thompson, D. L. *J. Phys. Chem.*, submitted.

(5) Russell, T. P.; Miller, P. J.; Piermarini, G. J.; Block, S.; Gilardi, R.; George, C. *AD-CO48 931 (92−0134)*; CPIA Abstract No. 92, 0149. ADD604 542, C-D, Chemical Propulsion Information Agency: Columbia, MD, 1991; p 155.

(6) McCrone, W. C. In *Physics and Chemistry of the Organic Solid State*; Fox, D., Labes, M. M., Weissberger, A., Eds.; Wiley: New York, 1965; Vol. II, pp 726−766.

(7) Breneman, C. M.; Wiberg, K. B. *J. Comput. Chem*. **1990**, *11*, 361.

(8) Hehre, W.; Radom, L.; Schleyer, P. v. R.; Pople, J. A. *Ab Initio Molecular Orbital Theory*; Wiley-Interscience: New York, 1986.

(9) Möller, C. M. S. *Phys. Rev*. **1934**, *46*, 618. Hehre, W. J.; Ditchfield, R.; Pople, J. A. *J. Chem. Phys*. **1972**, *56*, 2257. Hariharan, P. C.; Pople, J. A. *Theor. Chim. Acta* **1973**, *28*, 213. Gordon, M. S. *Chem. Phys. Lett*. **1980**, *76*, 163.

(10) Hohenber, P.; Kohn, W. *Phys. Rev. B* **1964**, *126*, 864. Parr, R. G.; Yand, W. *Density-Functional Theory of Atoms and Molecules*; Oxford University Press: New York, 1989.

(11) Frisch, M. J.; Trucks, G. W.; Schlegel, H. B.; Gill, P. M. W.; Johnson, B. G.; Robb, M. A.; Cheeseman, J. R.; Keith, T.; Patersson, G. A.; Montgomery, J. A.; Raghavachari, K.; AL-Laham, M. A.; Zakrzewski, V. G.; Ortiz, J. V.; Foresman, J. B.; Cioslowski, J.; Stefanov, B. B.; Nanyakkara, A.; Challacombe, M.; Peng, C. Y.; Ayala, P. Y.; Chen, W.; Wong, M. W.; Andres, J. L.; Replogle, E. S.; Gomperts, R.; Martin, R. L.; Fox, D. J.; Binkley, J. S.; Defrees, D. J.; Baker, J.; Stewart, J. P.; Head-Gordon, M.; Gonzales, C.; Pople, J. A. *Gaussian 94*, revision C.3; Gaussian, Inc.; Pittsburgh, PA, 1995.

(12) Becke, A. D. *J. Chem. Phys*. **1993**, *98*, 5648.

(13) Lee, C.; Yang, W.; Parr, R. G. *Phys. Rev*. **1988**, *B41*, 785.

(14) Hariharan, P. C.; Pople, J. A. *Theor. Chim. Acta* **1973**, *28*, 213.

(15) Cox, S. R.; Williams, D. E. *J. Comput. Chem*. **1981**, *2*, 304.

(16) Price, S. L.; Andrews, J. S.; Murray, C. W.; Amos, R. D. *J. Am. Chem. Soc*. **1992**, *114*, 8268.

(17) Coombes, D. S.; Price, S. L.; Willock, D. J.; Leslie, M. *J. Phys. Chem*. **1996**, *100*, 7352.

(18) Pertsin, A, J.; Kitaigorodsky, A. I. *The Atom-Atom Potential Method, Applications to Organic Molecular Solids*; Springer-Verlag: Berlin, 1987.

(19) Desiraju, G. R. *Crystal Engineering*: *The Design of Organic Solids*; Elsevier: Amsterdam, 1989.

(20) Williams, D. E. *Acta Crystallogr*. **1977**, *A27*, 452.

(21) Williams, D. E. In *Crystal Cohesion and Confirmational Energies*; Metzger, R. M., Ed.; Springer-Verlag: Berlin, 1981; pp 3−40.
(22) Williams, D. E. *PCK91, A Crystal Molecular Packing Analysis Program*; Department of Chemistry, University of Louisville: Louisville, KY.
(23) Starr, T. L.; Williams, D. E. *Acta Crystallogr.* **1977**, *A33*, 771.
(24) Sorescu, D. C.; Thompson, D. L. *J. Phys. Chem. B* **1997**, *101*, 3605.
(25) Gibson, K. D.; Scheraga, H. A. *J. Phys. Chem.* **1995**, *99*, 3752.
(26) Gibson, K. D.; Scheraga, H. A. *LMIN: A Program for Crystal Packing*; QCPE No. 664.
(27) *International Tables for Crystallography*; Hahn, T., Ed.; Reidel: Dordrecht, 1983.
(28) *Fundamentals of Crystallography*; Giacovazzo, C., Ed.; Oxford University Press: New York, 1992.
(29) Nosé, S.; Klein, M. L. *Mol. Phys.* **1983**, *50*, 1055.
(30) Smith, W. *MDSCPC4B, A Program for Molecular Dynamics Simulations of Phase Changes*; CCP5 Program Library (SERC), 1991.
(31) Allen, M. P.; Tindesley, D. J. *Computer Simulation of Liquids*; Oxford University Press: New York, 1989.
(32) Allen, F. H.; Kennard, O.; Watson, D. G.; Brammer, L.; Orpen, A. G.; Taylor, R. *J. Chem. Soc., Perkin Trans. 2* **1987**, S1−S19.
(33) Allen, F. H.; Kennard, O. *Chem. Des. Autom. News* **1993**, *8*, 31.
(34) (1) Trideuteronitromethane (NTROMA13). (2) Trinitromethane (HEVRUV). (3) 1,2-Dinitroethane (JUTGEK). (4) 2,3-Dimethyl-2,3-dinitrobutane (BECJEY). (5) Hexanitroethane (QQQBRD02). (6) 1,1,1,3,5,5,5-Heptanitropentane (CUVXOG). (7) 1,1,1,3,3,5,5,5-Octanitropentane (CEYDUF). (8) *trans*-1,2-Dinitrocyclopropane (FOHMUK). (9) *trans*-1,2-Dinitro(2.2)spiropentane (JOHBUD01). (10) 1,1′-Dinitrobicyclopropyl (BECJIC). (11) 1,1,3,3-Tetranitrocyclobutane (VUCBAW). (12) 1,1′-Dinitrobicyclobutyl (BECJUO). (13) 1,3,5-Trinitrobenzene (TNBENZ10). (14) 2,4,6-Trinitrotoluene, orthorhombic form. (15) 2,4,6-Trinitrotoluene, monoclinic form. (16) 2,2′,4,4′,6,6′-Hexanitrostilbene (GIMBOT). (17) 1,1,4,4-Tetranitrocyclohexane (JUVNAP). (18) 1,2,3-Trimethyl-r-3,c-4,c-6-trinitro-t-5-trinitromethylcylohex-1-ene (ZORHUJ). (19) 1,8-Dinitronaphthalene (DNTNAP01). (20) 1,4-Dinitrocubane (CEDZUG). (21) 1,3,5-Trinitrocubane (HASHAK). (22) 1,3,5,7-Tetranitrocubane (HASHEO). (23) 1,2,3,5,7-Pentanitrocubane (NACXEU). (24) 2,2,5,5-Tetranitrobicyclo-(2.2.1)heptane (JUVMIW). (25) 3,7-Dinitronoradamantane (LINHUL). (26) 3,7,9-Trinitronoradamantane (LINJAT). (27) 2,2-Dinitroadamantane (CAXNIY). (28) 1,3,5,7-Tetranitroadamantane (BUYPUG10). (29) 2,2,4,4-Tetranitroadamantane (TAFDUZ). (30) 8,8,11,11-Tetranitropentacyclo-(5.4.0.0.^{2,6}0.^{3,10}0^{5,9})undecane (VIKYUJ). (31) 2,6-Dinitro-hexacyclo-(5.4.1.0.^{2,6}0.^{3,10}0.^{5,9}0^{8,11})dodecane (DAFWAI). (32) Decahydro-2,2,5,5-tetranitro-1,6:3,4-dimethanocyclobuta(1,2:3,4)dicyclopentene (LEJKOA). (33) 5,5,11-Trinitrohexacyclo(5.4.1.0.^{2,6}0.^{3,10}0.^{4,8}0^{9,12})dodecane Trinitro-1,3-bis(homopentaprismane) (DUYREU). (34) 5,5,11,11-Tetranitrohexacyclo-(5.4.1.0.^{2,6}0.^{3,10}0.^{4,8}0^{9,12})dodecane (DUYRIY). (35) 6,6,10,10-Tetranitropentacyclo(5.3.0.0.^{2,5}0.^{3,9}0^{4,8})decane (DAFGAS). (36) 4,4,8,8,11,11-Hexanitropentacyclo(5.4.0.0.^{2,6}0.^{3,10}0^{5,9})undecane (JAJBEB). (37) *m*-Nitrophenol, monoclinic form (MNPHOL02). (38) 2,4-Dinitrophenol (DNOPHL01). (39) 2,4,6-Trinitrophenol (picric acid) (PICRAC11). (40) *N,N*-Dimethyl-2,4,6-trinitroaniline (JUPRIV). (41) 6-Methyl-2-nitrobenzonitrile (ZUGPOG). (42) 2,6-Dinitrobenzonitrile (ZUGPOJ). (43) 1,4-Diacetyl-3,6-dinitrotetrahydroimidazo-(4,5-d)imidazole-2,5(1H,3H)-dione, 3,6-Diacetyl-1,4-dinitroglycoluril (DEFLEF). (44) 5,7-Dinitro-1-picrylbenzotriazole (PABBOJ). (45) 2-Nitro-6,7,8,9-tetrahydronaphtho(2,1-b)furan (DETDOV). (46) 3,6-Dimethyl-c-5-nitrato-1,r-3,t-4,c-6-tetranitrocyclohexene (KIJNUM). (47) 3-Nitrato-1-nitroazetidine (VUBZUN). (48) 1-Methoxymethoxy-3,5-dinitrobenzene (DEMSOD). (49) 1,2,3-Propanetriol trinitrate, β-modification (CORYIR). (50) Pentaerythritol tetranitrate (PETN), form I (PERYTN10). (51) Pentaerythritol tetranitrate, form II (PERYTN01).
(35) (1) Trevino, S. F.; Prince, E.; Hubbard, C. R. *J. Chem. Phys.* **1980**, *73*, 2996. (2) Schodel, H.; Dienelt, R.; Bock, H. *Acta Crystallogr.* **1994**, *C50*, 1790. (3) Lam, Y.-L.; Koh, L. L.; Huang, H. H. *J. Chem. Soc., Perkin Trans.* **1993**, *2*, 175. (4) Kai, Y.; Knochel, P.; Kwiatkowski, S.; Dunitz, J. D.; Oth, J. F. M.; Seebach, D.; Kalinowski, H.-O. *Helv. Chim. Acta* **1982**, *65*, 137. (5) Bougeard, D.; Boese, R.; Polk, M.; Woost, B.; Schrader, B. *J. Phys. Chem. Solids* **1986**, *47*, 1129. (6) Atovmyan, L. O.; Golovina, N. I.; Eremenko, L. T.; Zhitomirskaya, N. G.; Oreshko, G. V.; Fadeev, M. A. *Izv. Akad. Nauk SSSR, Ser. Khim.* **1984**, 549. (7) Eremenko, L. T.; Atovmyan, L. O.; Golovina, N. I.; Oreshko, G. V.; Fadeev M. A. *J. Chem. Soc., Chem. Commun.* **1984**, 709. (8) Wade, P. A.; Dailey, W. P.; Carroll, P. J. *J. Am. Chem. Soc.* **1987**, *109*, 5452. (9) Marsh, R. E. *Acta Crystallogr. B* **1997**, *53*, 317. (10) See (4). (11) Gilardi, R.; George, C.; Flippen-Anderson, J. L. *Acta Crystallogr. C* **1992**, *48*, 1680. (12) See (4). (13) Choi, C. S.; Abel, J. E. *Acta Crystallogr.* **1972**, *B28*, 193. (14) Carper, W. R.; Davis, L. P.; Extine, M. W. *J. Phys. Chem.* **1982**, *86*, 459. (15) Duke, J. R. C. Private communication, 1971. (16) Gerard, F.; Hardy, A. *Acta Crystallogr. C* **1993**, *44*, 1283. (17) Olah, G. A.; Ramaiah, P.; Prakash, G. K. S.; Gilardi, R. *J. Org. Chem.* **1993**, *58*, 763. (18) Butts, C. P.; Eberson, L.; Hartshorn, M. P.; Robinson, W. T.; Timmerman-Vaughan, D. J.; Young, D. A. W. *Acta Chem. Scand.* **1996**, *50*, 29. (19) Ciechanowicz-Rutkowska, M. *J. Solid State Chem.* **1977**, *22*, 185. (20) Eaton, P. E.; Ravi Shankar, B. K.; Price, G. D.; Pluth, J. J.; Gilbert, E. E.; Alster, J.; Sandus, O. *J. Org. Chem.* **1984**, *49*, 185. (21) Eaton, P. E.; Xiong, Y.; Gilardi, R. *J. Am. Chem Soc.* **1993**, *115*, 10195. (22) See (21). (23) Lukin, K.; Li, J.; Gilardi, R.; Eaton, P. E. *Angew. Chem., Int. Ed. Engl.* **1996**, *35*, 864. (24) See (17). (25) George, C.; Gilardi, R. D.; Zajac, W. W., Jr.; Buzby, J. H.; Walters, T. R. *Acta Crystallogr. C* **1995**, *51*, 703. (26) See (25). (27) George, C.; Gilardi, R. *Acta Crystallogr. C* **1983**, *39*, 1674. (28) George, C.; Gilardi, R. *Acta Crystallogr. C* **1984**, *40*, 674. (29) Dave, P. R.; Ferraro, M.; Ammon, H. L.; Choi, C. S. *J. Org. Chem.* **1990**, *55*, 4459. (30) Flippen-Anderson, J. L.; George, C.; Gilardi, R.; Zajac, W. W., Jr.; Walters, T. R.; Marchand, A.; Dave, P. R.; Arney, B. E., Jr. *Acta Crystallogr. C* **1991**, *47*, 813. (31) Paquette, L. A.; Fischer, J. W.; Engel, P. *J. Org. Chem.* **1985**, *50*, 2524. (32) Ammon, H. L.; Du, Z.; Holden, J. R.; Paquette, L. A. *Acta Crystallogr. B* **1994**, *50*, 216. (33) Paquette, L. A.; Nakamura, K.; Engel, P. *Chem. Ber.* **1986**, *119*, 3782. (34) See (33). (36) George, C.; Gilardi, R.; Flippen-Anderson, J. L.; Choi, C. S.; Marchand, A. P.; Reddy, D. S. *Acta Crystallogr. C* **1985**, *41*, 788. (36) Marchand, A. P.; Dave, P. R.; Rajapaksa, D.; Arney, B. E., Jr.; Flippen-Anderson, J. L.; Gilardi, R.; George, C. *J. Org. Chem.* **1989**, *54*, 1769. (37) Pandarese, F.; Ungaretti, L.; Coda, A. *Acta Crystallogr. B* **1975**, *31*, 2671. (38) Iwasaki, K.; Kawano, Y. *Acta Crystallogr. B* **1977**, *33*, 2455. (39) Srikrishnan, T.; Soriano-Garcia, M.; Parthasarathy, R. *Z. Kristallogr.* **1980**, *151*, 317. (40) Butcher, R. J.; Gilardi, R.; Flippen-Anderson, J. L.; George, C. *New J. Chem.* (*Nouv. J. Chim.*) **1992**, *16*, 679. (41) Britton, D.; Cramer, C. J. *Acta Crystallogr. B* **1996**, *52*, 344. (42) See (41). (43) Boileau, J.; Wimmer, E.; Pierrot, M.; Baldy, A.; Gallo, R. *Acta Crystallogr. C* **1985**, *41*, 1680. (44) Flippen-Anderson, J. L.; Gilardi, R. D.; Pitt, A. M.; Wilson, W. S. *Aust. J. Chem.* **1992**, *45*, 513. (45) Bideau, J.-P.; Bravic, G.; Cotrait, M. *Acta Crystallogr. C* **1985**, *41*, 1799. (46) Abell, A. D.; Hartshorn, M. P. M.; Maclennan, E.; Robinson, W. T.; Wright, G. J. *Aust. J. Chem.* **1991**, *44*, 43. (47) See (11). (48) Jones, P. G.; Sheldrick, G. M.; Kirby, A. J.; Briggs, A. J. *Acta Crystallogr. C* **1985**, *41*, 1377. (49) Espenbetov, A. A.; Antipin, Yu. M.; Struchkov, Yu. T.; Philippov, V. A.; Tsirel'son, V. G.; Ozerov, R. P.; Svetlov, B. S. *Acta Crystallogr. C* **1984**, *40*, 2096. (50) Trotter, J. *Acta Crystallogr.* **1963**, *16*, 698. (51) Cady, H. H.; Larson, A. C. *Acta Crystallogr. B* **1975**, *41*, 1864.
(36) (a) Chickos, J. S. In *Molecular Structure and Energetics*; Liebman, J. F., Greenberg, A., Eds.; VCH Publishers Inc.: New York, 1987; Vol. 2. (b) Pepekin, V. I.; Miroshnichenko, E. A.; Lebedev, Yu. A.; Apin, A. Ya. *Russ. J. Phys. Chem.* (Engl. Transl.) **1968**, *42*, 1583. (c) Cundall, R. B.; Palmer, T. F.; Wood, C. E. C. *J. Chem. Soc. Faraday Trans.* I **1978**, *74*, 1339. (d) Edwards, G. *Trans. Faraday Soc.* **1950**, *46*, 423. (e) Fritzsche, K.; Dogan, B.; Beckhaus, H.-D.; Ruechardt, C. *Thermochim. Acta* **1990**, *160*, 147. (f) Wolf, K. L.; Weghofer, H. *Z. Phys. Chem. B* 1938, *39*, 194. (g) Hoyer, H.; Peperle, W., *Z. Electrochem.* **1958**, *62*, 61. (h) Edwards, G. *Trans. Faraday. Soc.* **1953**, *49*, 152.
(37) Gallagher, H. G.; Roberts, K. J.; Sherwood, J. N.; Smith, L. A *J. Mater. Chem.* **1997**, *7*, 229 and references therein.
(38) Graber, D. G.; Rauch, F. C.; Fanelli, A. J. *J. Phys. Chem.* **1969**, *73*, 3514.
(39) Blomquist, A. T.; Ryan, J. F., Jr. *Studies Related to the Stability of PETN*; OSRD Report NDRC-B-2566, 1944.
(40) Dobratz, M. *Properties of Chemical Explosives and Explosive Simulants*; Lawrence Livermore National Laboratory: Livermore, CA; Report UCRL-52997, 1981.
(41) Cady, H. H. *J. Chem. Eng. Data* **1972**, *17*, 369.